

Ultrafast Dynamics of Nano and Mesoscopic Systems Driven by Asymmetric Electromagnetic Pulses

A. Matos-Abiague, A. S. Moskalenko, and J. Berakdar

Max-Planck-Institut für Mikrostrukturphysik, Weinberg 2, 06120 Halle, Germany

This work provides an overview on the theoretical description of the electron dynamics in nano and mesoscopic semiconductor structures driven by short asymmetric electromagnetic pulses. For double quantum well structures we show how the electron can be steered within picoseconds into certain spatial regions and discuss ways to maintain in time this non-stationary situations. We also show how charge polarization and charge current can be swiftly generated in mesoscopic rings when irradiated with electromagnetic pulses. We also envisage the possibility of pulse-induced electron removal from quantum dots.

Keywords: 78.67.-n, 42.65.Ky, 42.65.Re

1. Introduction

The everlasting development in the generation and engineering of short laser pulses [1] is giving rise to an increasing number of their utilization in tracing in time the response and the transitions of matter between various states. Even subfemto second resolution has become available which opens the way for exploring the dynamics of new fundamental physical, chemical, and biological processes [2]. Another exciting development in fast optical probes is the generation of strongly asymmetric monocycle linearly (or circularly) polarized electromagnetic pulses [3], often called half-cycle (HCPs) for the reason which will become obvious below. The time structure of the electric field amplitude of an HCP is shown in Fig.1. It consists of a very short, strong half-cycle (it is in fact this part which is referred to as an HCP), followed by a second long and a much weaker half-cycle of an opposite polarity (the tail of the HCP) [4].

A method for generating HCPs is the following (cf. Fig.1): a wafer of biased gallium-arsenide (GaAs) semiconductor is irradiated by a short pulse from a Ti:Sapphire chirped-pulse amplifier. The wafer is photoconductive with a band gap of ~ 1.4 eV. Upon the illumination of one side of the

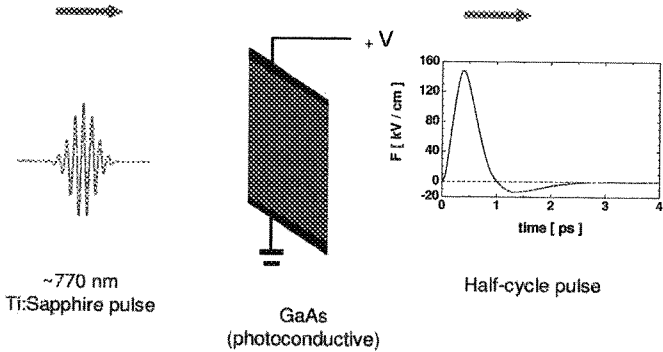


Fig. 1. The method for the generation of half-cycle pulses, as reported in [3].

wafer with the ca. 770 nm laser pulse the GaAs wafer turns conductive and the electrons are quickly accelerated and radiate a short unipolar coherent electromagnetic pulse. The polarization axis is in the direction of the bias field. The strength of the HCP depends linearly on the bias field strength. The relaxation of GaAs wafer to the insulating ground state following the excitation process occurs on a much longer time scale (hundreds of picoseconds) which leads to the extended tail of the HCP (with opposite polarity). Experimentally realized HCPs have an amplitude asymmetry ratio of 13 : 1 between the HCP peak field and peak tail. [3]. Reported HCPs possess peak fields of up to several hundreds of kV/cm and have a duration in the range between nanosecond and subpicoseconds.

2. Theoretical considerations

The purpose of this work is to expose the nature of the electron dynamics driven by HCPs. To highlight the features akin to the interaction of an HCP with charged particles let us consider a general system described by the Hamiltonian $H^{(0)}$ which is subjected at $t = t_1$ to an electromagnetic pulse. The system propagates as prescribed by the time-evolution operator $U(t, 0)$ which satisfies the equation of motion

$$i\hbar \frac{\partial U(t, 0)}{\partial t} = [H^{(0)} + V(t)]U(t, 0) . \quad (1)$$

$V(t)$ describes the interaction of the pulse with the system.

For the time-evolution operator the following relations apply

$$U(t, 0) = U_0(t, t_1)U(t, t_1, 0)U_0(t_1, 0), \quad (2)$$

$$U(t, t_1, 0) = U_0^\dagger(t, t_1)U(t, 0)U_0^\dagger(t_1, 0), \quad (t > t_1). \quad (3)$$

Here $U_0(t, t_1)$ is the evolution operator of the undriven system. From Eqs. (1) and (2) we deduce that

$$U(t, t_1, 0) = \hat{T} \exp \left[-\frac{i}{\hbar} \int_{-t_1}^{t-t_1} e^{iH^{(0)}t'/\hbar} V(t' + t_1) e^{-iH^{(0)}t'/\hbar} dt' \right], \quad (4)$$

where \hat{T} is the time-ordering operator. In what follows we will be dealing with systems with a relevant characteristic time scale being much longer than the duration of the HCP. In such a case, i.e. for a short interaction time, the time ordering in Eq. (4) becomes irrelevant, and the propagator is cast as (this approximation amounts to the first order in the Magnus expansion of the exponential [5])

$$U(t, t_1, 0) = \exp \left[-\frac{i}{\hbar} \int_{-t_1}^{t-t_1} e^{iH^{(0)}t'/\hbar} V(t' + t_1) e^{-iH^{(0)}t'/\hbar} dt' \right]. \quad (5)$$

Noting that

$$e^{-A} B e^A = B + [B, A] + \frac{1}{2!} [(B, A), A] + \dots, \quad (6)$$

we derive the following expansion for the propagator

$$U(t, t_1, 0) = \exp \left[-\frac{i}{\hbar} V_0 + \frac{i}{\hbar^2} [V_1, iH^{(0)}] + \frac{i}{2!\hbar^3} \{ [V_2, H^{(0)}], H^{(0)} \} + \dots \right], \quad (7)$$

$$V_n = \int_0^t (t' - t_1)^n V(t') dt', \quad n = 0, 1, 2, \dots \quad t > t_1. \quad (8)$$

2.1. The impulsive approximation

Let us assume the interaction potential $V(t)$ to have, in the configuration space, the form

$$V(t) = \mathbf{r} \cdot \mathbf{e} F a(t - t_1),$$

where \mathbf{r} is the position coordinate of the driven charge and \mathbf{e} is the external-field polarization vector. F is the peak amplitude of the field. The time envelope of the pulse we denote by $a(t - t_1)$. E.g., if the pulse has a Gaussian form we write

$$a(t - t_1) = \exp[-(t - t_1)^2 / (2\sigma^2)].$$

For pulses strongly peaked at t_1 we conclude that

$$V_0 = \mathbf{r} \cdot \mathbf{e} F \sigma \sqrt{2\pi} \quad , \quad V_1 = 0 \quad , \quad V_2 = V_0 \sigma^2 \quad . \quad (9)$$

The relevance of the various terms in the exponential appearing in Eq. (7) depends decisively on the parameters of the external fields. For example, if the duration of the HCP, quantified by σ is much smaller than the characteristic time of the system τ_c , estimated by $\Delta\epsilon/\hbar \sim \tau_c^{-1}$ (where $\Delta\epsilon$ is the level spacing near the ground state) then the first term of the expansion in Eq. (7) dominates and the propagator (Eq. (7)) reduces to the form

$$U(t, t_1, 0) = \exp \left[\frac{i}{\hbar} \mathbf{r} \cdot \mathbf{p} \right] \quad . \quad (10)$$

Here the vector \mathbf{p} plays the role of a momentum and is evaluated as the time-integral over the pulse, i.e.

$$\mathbf{p} = -\mathbf{e} F \int_{-\infty}^{\infty} a(t') dt' \quad . \quad (11)$$

Within this sudden-excitation limit (also called the impulsive approximation (IA)) the evolution operator has then the final form

$$U(t, 0) = U_0(t, t_1) e^{\frac{i}{\hbar} \mathbf{r} \cdot \mathbf{p}} U_0(t_1, 0) \quad . \quad (12)$$

According to this finding the pulse delivers an instantaneous *kick* to the system accompanied by a transfer of the momentum \mathbf{p} . The particle's wave functions just before ($t = t_1^-$), and right after ($t = t_1^+$) the interaction with the pulse are interrelated via the condition

$$\Psi(\mathbf{r}, t_1^+) = e^{\frac{i}{\hbar} \mathbf{r} \cdot \mathbf{p}} \Psi(\mathbf{r}, t_1^-) \quad . \quad (13)$$

This relation tells that the system evolves in a field-free manner in between the kicks. This does not mean however that the system upon the pulse is in a stationary state, as shown in full details below.

3. Electron localization and dynamical control in semiconductor double quantum wells

As an illustration let us consider the dynamics of the charge carriers confined in a double quantum well (DQW) as typically formed in $\text{Al}_x\text{Ga}_{1-x}$ As structures. Within the parabolic band and the effective mass approximations (the effective mass $m^* = 0.067m_0$) the particle moves in an effective potential V_{conf} which has the form plotted in Fig. 2 (a). The particle is then subjected to a sequence of HCPs as schematically shown in Fig. 2 (b), i.e.

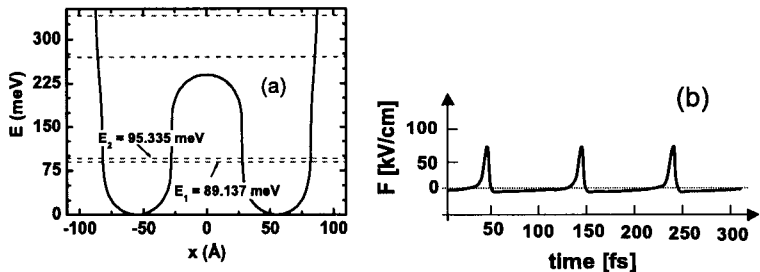


Fig. 2. (a) The confining potential V_{conf} of the charge carrier, as used in the text. The central barrier height is ~ 240 meV. The dashed lines point to the first lowest energy levels. (b) The electric field amplitude vs. time for the sequence of HCPs acting on the particle in (a).

$$V(x, t) = x \sum_{k=0}^{N_p-1} F_k a(t - t_p - t_k) , \quad (14)$$

where

$$a(t) = \begin{cases} \exp\left[-\frac{t^2}{2\sigma^2}\right] \cos \Omega t & \text{if } -\frac{\pi}{2\Omega} \leq t < T - \frac{\pi}{2\Omega} \\ 0 & \text{otherwise} \end{cases} . \quad (15)$$

Here F_k stands for the peak field of the k -th pulse, $t_p = \frac{\pi}{2\Omega}$ corresponds to the time at which the positive tail of the first applied pulse is centered, T is the time between consecutive pulses, N_p is the number of applied pulses, and σ characterizes the width of the pulses. The parameter $\Omega = \frac{\pi}{3\sigma\sqrt{\ln 2}}$ in Eq. (15) guarantees a ratio 8:1 between the peak amplitudes of the positive and negative tails of the pulses. The duration d of the positive tail of each pulse is given by $d = 3\sigma\sqrt{\ln 2}$ (in the calculations presented below we use $\sigma = 20$ fs).

In the ground state the particle is delocalized, i.e. it has the same probability to be in the left or in the right well. Here we are interested in the possibility of localizing the electron in one of the wells upon the application of the HCPs. The localization can be quantified by the time-dependent probability

$$P_L(t) = \int_{-\infty}^0 \Psi^*(x, t) \Psi(x, t) dx \quad (16)$$

which is the probability of finding the particle in the left well. We apply at the time $t = t_p$ a pulse with a strength F_{aux} that creates a time-dependent coherent state. We then pose the question of which kind of sequence of

pulses is needed to localize the particle in one of the well upon the time period $t = t_p + t_{loc}$. Here t_{loc} is the localization time.

For an insight into the possible solution to this task let us consider excitations restricted to the two lowest-energy levels only, i.e. we reduce at first the system to a two-level system. Furthermore, we note that the characteristic time $\tau_c = 2\pi/\omega_c$ where ω_c is the frequency corresponding to the energy difference between the ground and the first excited states of the field-free quantum well, is on the range of $\tau_c \approx 665$ fs. On the other hand the pulses we will apply have a duration of ~ 80 fs. As explained in the preceding section we can utilize in this case the impulsive approximation for the time evolution upon excitation.

The wave function of the system is cast in terms of the wave functions $\Psi_n^{(0)}(x)$ ($n = 1, 2$) of the two unperturbed lowest levels, i.e.

$$\Psi(x, t) = \sum_{n=1}^2 C_n(t) \Psi_n^{(0)}(x) . \quad (17)$$

Here the expansion coefficients $C_n(t)$ are expressible in terms of a two-dimensional spinor $\mathbf{C}(t) = (C_1(t), C_2(t))^T$ whose dynamics is governed by the time-dependent Schrödinger equation

$$i\hbar \frac{\partial \mathbf{C}(t)}{\partial t} = \left[-(\hbar\omega_c/2)\sigma_z + \mu_{12} \sum_{k=0}^{N_p-1} F_k a(t - t_p - t_k) \sigma_x \right] \mathbf{C}(t) . \quad (18)$$

σ_x and σ_z are Pauli matrices and the transition dipole is introduced as $\mu_{12} = \langle \Psi_1^{(0)}(x) | x | \Psi_2^{(0)}(x) \rangle$.

From Eqs. (16) and (17) we deduce that

$$P_L(t) = \frac{1}{2} + \text{Re}[C_1^*(t)C_2(t)] . \quad (19)$$

Once the pulse is applied at $t = t_p$ the spinor $\mathbf{C}(t) = (C_1(t), C_2(t))^T$ transforms in time as

$$\mathbf{C}(t) = U_0(t, t_p) U(t, t_p, 0) U_0(t_p, 0) \mathbf{C}(0) , \quad (20)$$

$$U_0(t, t') = \begin{pmatrix} e^{\frac{i}{2}\omega_c(t-t')} & 0 \\ 0 & e^{-\frac{i}{2}\omega_c(t-t')} \end{pmatrix} , \quad (21)$$

$$U(t, t_p, 0) = e^{\frac{i}{\hbar} p_0 \sigma_x} = \begin{pmatrix} \cos\left(\frac{\mu_{12} p_0}{\hbar}\right) & i \sin\left(\frac{\mu_{12} p_0}{\hbar}\right) \\ i \sin\left(\frac{\mu_{12} p_0}{\hbar}\right) & \cos\left(\frac{\mu_{12} p_0}{\hbar}\right) \end{pmatrix} , \quad (22)$$

$$p_0 = p_{aux} = F_{aux} \int_{-\infty}^{\infty} a(t - t_p) dt . \quad (23)$$

If we start with the initial condition $\mathbf{C}(t) = (1, 0)^T$, i.e. from the ground state, Eqs. (19) - (22) tell us that if the pulse has a peak amplitude

$$\mu_{12} p_0 / \hbar = \pi/4 \quad (24)$$

the probability to be in the left well becomes

$$P_L(t_p + \tau_c/4) = 1.$$

This means $\tau_c/4$ is the time it takes for the electron to localize in the left well (within the IA and the two-level approximation). The localization peak field is then determined by Eqs. (23) and (24) This localization phenomenon is not sustainable without the application of additional, appropriately designed fields. To achieve time sustainability one may apply for example a train of HCPs with a period T at the time $t_1 = t_p + \tau_c/4 + \gamma$, $\gamma \ll \tau_c/4$ (here we assume $F_k = F$, $k = 1, 2, \dots, N_p - 1$). The system evolution at stroboscopic times $t = t_1 + (k - 1)T$; $k = 1, \dots, N_p - 1$ follows the relation

$$\mathbf{C}(t_1 + (k - 1)T) = [U(t_1 + T, t_1)]^{k-1} \mathbf{C}(t_1) \quad ; \quad k = 1, \dots, N_p - 1 \quad , \quad (25)$$

$$\begin{aligned} U(t_1 + T, t_1) &= U_0(t_1 + T, t_1)U(t_1 + T, t_1, t_1) \\ &= \begin{pmatrix} e^{\frac{i}{2}\omega_c T} \cos\left(\frac{\mu_{12} p}{\hbar}\right) & ie^{\frac{i}{2}\omega_c T} \sin\left(\frac{\mu_{12} p}{\hbar}\right) \\ ie^{-\frac{i}{2}\omega_c T} \sin\left(\frac{\mu_{12} p}{\hbar}\right) & e^{-\frac{i}{2}\omega_c T} \cos\left(\frac{\mu_{12} p}{\hbar}\right) \end{pmatrix} , \end{aligned} \quad (26)$$

$$p = F \int_{-\infty}^{\infty} a(t - t_1) dt . \quad (27)$$

Now we drive the system periodically such that it undergoes a cyclic evolution, for the spinor vectors this means that

$$\mathbf{C}(t_1 + lT) = e^{i\phi_l} \mathbf{C}(t_1) \quad ; \quad l = 0, 1, 2, \dots . \quad (28)$$

The real phase ϕ_l is gained by the wave function upon the l th evolution cycle that has a duration of T . The key point is that for periodic cyclic evolution $P_L(t)$ turns periodic with period T

$$P_L(t_1 + lT) = P_L(t_1) \quad ; \quad l = 0, 1, 2, \dots . \quad (29)$$

So if $P_L(t_1) \approx 1$ the particle localizes also in the left well at any time $t = t_1 + lT$. From Eqs. (25)-(28) we conclude that for peak amplitudes such that

$$\mu_{12} p / \hbar = (2n + 1)\pi/2; \quad n \in \mathbb{Z} \quad (30)$$

the system undergoes a cyclic evolution with [6]

$$\mathcal{T} = T \quad \text{if} \quad \gamma = T/2, \quad (31)$$

$$\text{or} \quad \mathcal{T} = 2T \quad \text{if} \quad \gamma \neq T/2. \quad (32)$$

The peak amplitudes $F_k = F$ suitable for the suppression of the electron tunnelling are then determined by Eqs. (27) and (30).

3.1. Numerical illustrations

Here we present two types of calculations: One type of calculations is based on the above analytical results for the two-level systems and the second derives from the full-numerical solution (including all levels). Figs. 3(a) and (b) show the time dependence of P_L whereas Fig. 3(c) shows the average probability $\langle P_L \rangle_{\tau_s} = (1/\tau_s) \int_0^{\tau_s} P_L(t) dt$ for $\tau_s = 2$ ps as a function of the pulse amplitude. Fig. 3(c) evidences that the localized particle can be displaced in controllable way in between the wells by tuning the pulse amplitudes.

Once the particle has been localized in one of the well we can, as we explained above, sustain this localization by applying a train of HCPs with a period $T \ll \tau_c/4$. An example of such a case is shown in Fig. 4 where a strong and a sustainable localization is achieved for the field parameters displayed on the figures.

4. Driven electron dynamics in mesoscopic rings

A further example that we present here is the dynamics of phase-coherent electrons confined in mesoscopic rings (MRs). Such systems have served for the demonstration of a variety of fundamental phenomena [7–13] such as the Aharonov-Bohm effect [14] and the appearance of persistent currents [15] when pierced by a magnetic flux. A number of studies have dealt with the electron-electron interaction [16–18], the impurity scattering [16] and disorder effects [11,17] on the persistent currents. Experimentally several measurements on persistent currents [15,19–21] have been conducted successfully. Furthermore, dynamical processes induced by a *time-dependent* electric field acting on a MR threaded by a static magnetic field have been investigated [22–25] in which case a stationary non-equilibrium current arises. This direct non-equilibrium current caused by nonlinear effects is however an odd function of the static magnetic flux and vanishes thus if the static magnetic flux is zero [23–25]. Studies on MRs subjected to external CW laser fields are reported in [26–28].

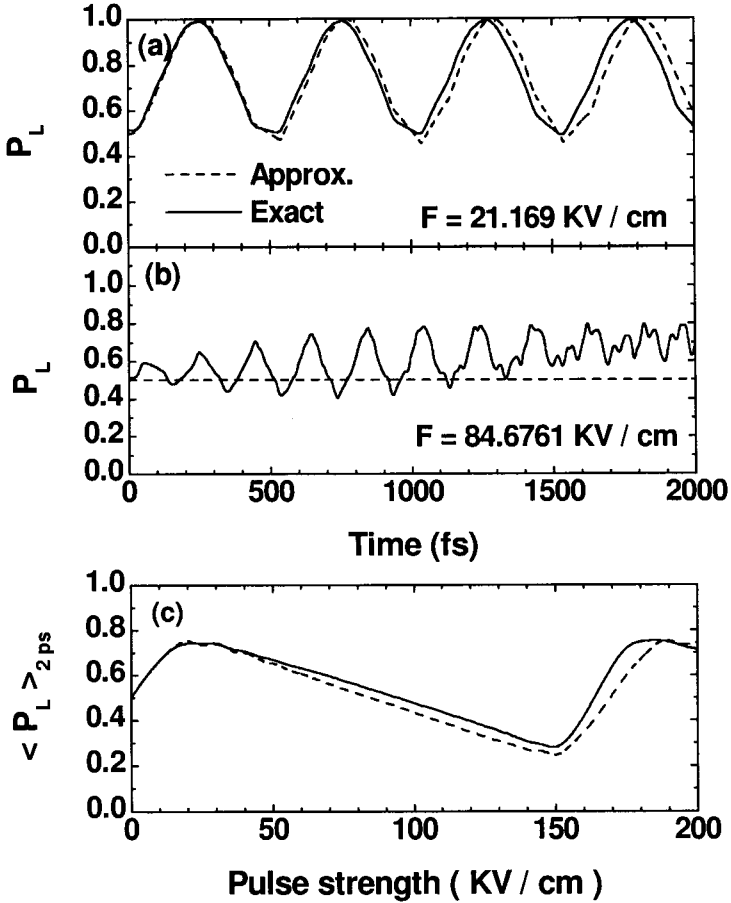


Fig. 3. (a) $P_L(t)$ for a pulse amplitude appropriate for the localization in one well. (b) Same as in (a) however the pulse amplitude is chosen such that the particle oscillates between the two wells. (c) P_L averaged over 2 ps as function of the pulse strength. Results of two-level approximation (dashed lines) and the results of full numerical calculations involving all the levels (solid lines) are shown.

Here we will be interested in the generation of nonequilibrium charge currents and charge polarization by means of HCPs [29]. Fig. 5 shows a schematics of the system to be studied here: An isolated ring with a width d and a radius $\rho_0 \gg d$ confines N charge carriers. The ring is subjected at the time $t = t_1$ to one or a train of HCPs that have an amplitude $F_1(t)$. As we will see below this pulse induces a non-equilibrium charge redistribution

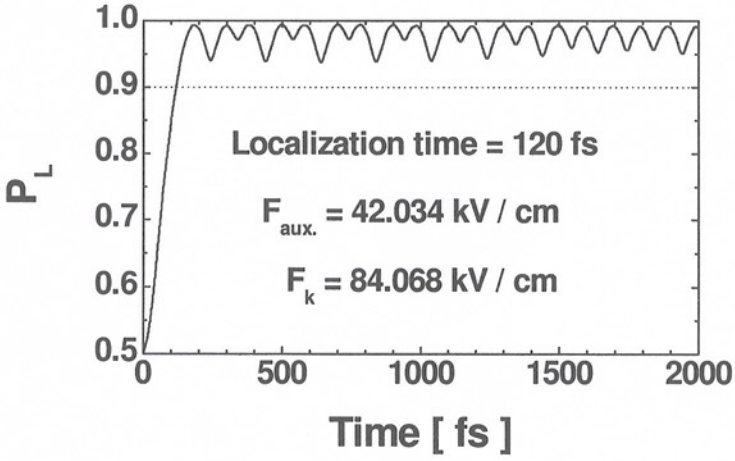


Fig. 4. P_L as a function of the time. After a pulse with $F_{aux} \approx 42$ kV/cm by a time delay $\tau = t_1 - t_p = 220$ fs we apply a train of HCPs with a period of $T = 100$ fs and peak amplitudes $F_k \approx 84.1$ kV/cm

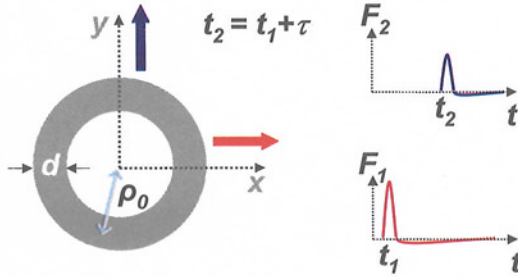


Fig. 5. A ballistic ring with a width d and a radius $\rho_0 \gg d$ subjected to a sequence of two crossed time-asymmetric pulses applied at $t = t_1$ and $t = t_2 = t_1 + \tau$. The pulses are linearly polarized along the perpendicular x and y axes, respectively.

in the ring, generating thus a charge polarization. However, it does not destroy the clockwise-anticlockwise symmetry of the charge density. We demonstrate further that charge currents can be generated if the ring is irradiated upon a time delay τ after the pulse F_1 by a second pulse $F_2(t)$. In this way clockwise-anticlockwise symmetry is broken and a time-dependent current $I(t)$ and an associated magnetization are induced.

4.1. Charge polarization buildup

For simplicity, we consider here a 1D ring. The influence of the radial channels can be incorporated in the model without much effort [29]. We concentrate on the case where the round trip time (few hundreds picoseconds) of the charge carriers in the MR is much longer than the pulse duration τ_d (picoseconds) in which case the IA is applicable. Thus, the wave function of the charge carrier with a charge q before and after the application of the HCP (that has the polarization axis along the x axis) are related via

$$\Psi(\theta, t = 0^+) = \Psi(\theta, t = 0^-) e^{i\alpha \cos \theta} , \quad (33)$$

where $\alpha = q\rho_0 p/\hbar$ and θ identifies the angular position of the charge carriers with respect to the x axis.

The function $\Psi_{m_0}(\theta, t)$ describes the dynamics of the particle that has started from the initial state labelled by orbital quantum number m_0 . $\Psi_{m_0}(\theta, t)$ can be expanded on the ring stationary eigenstates as

$$\Psi_{m_0}(\theta, t) = \frac{1}{\sqrt{2\pi}} \sum_{m=-\infty}^{\infty} C_m(m_0, t) e^{im\theta} e^{-i\frac{E_m t}{\hbar}} . \quad (34)$$

E_m are the stationary orbital energies of the unperturbed states, i.e.

$$E_m = \frac{\hbar^2 m^2}{2m^* \rho_0^2} , \quad m = 0, \pm 1, \pm 2, \dots . \quad (35)$$

From Eq. (33) we conclude for the expansion coefficients the relations

$$C_m(m_0, t) = \begin{cases} \delta_{m, m_0} & \text{for } t \leq 0 \\ i^{m_0 - m} J_{m - m_0}(\alpha) & \text{for } t > 0 \end{cases} , \quad (36)$$

where $J_l(x)$ are the Bessel functions [30]. The energy associated with a particle initially in the m_0 th state evolves as

$$\begin{aligned} E_{m_0}(t) &= \langle \Psi_{m_0}(\theta, t) | H | \Psi_{m_0}(\theta, t) \rangle, \\ &= i\hbar \left\langle \Psi_{m_0}(\theta, t) \left| \frac{\partial}{\partial t} \right| \Psi_{m_0}(\theta, t) \right\rangle . \end{aligned} \quad (37)$$

From Eqs. (34) - (36, 37) we find thus for $t > 0$

$$E_{m_0}(t > 0) = \frac{\hbar^2}{2m^* \rho_0^2} \sum_{m=-\infty}^{\infty} [m J_{m_0 - m}(\alpha)]^2 , \quad (38)$$

$$E_{m_0}(t) = \begin{cases} \frac{\hbar^2 m_0^2}{2m^* \rho_0^2} & \text{for } t \leq 0 \\ \frac{\hbar^2}{2m^* \rho_0^2} \left(m_0^2 + \frac{\alpha^2}{2} \right) & \text{for } t > 0 \end{cases} . \quad (39)$$

Recalling that $\alpha = q\rho_0 p/\hbar$ we arrive at the formula

$$E_{m_0}(t > 0) = E_{m_0}(t < 0) + \frac{q^2}{2} \frac{p^2}{2m^*}. \quad (40)$$

This relation indicates that the HCP shifts the unperturbed energy spectrum by an amount which scales quadratically with the pulse strength independently of the ring size. $E_{m_0}(t < 0)$ increases quadratically with m_0 so that the ring energy is virtually unchanged if $m_0^2 \gg \alpha^2$. To explore the possibility of creating charge polarization in the ring we study the quantity

$$\langle \cos \theta \rangle_{m_0}(t) = \int_0^{2\pi} |\Psi_{m_0}(\theta, t)|^2 \cos \theta d\theta, \quad (41)$$

which characterizes the charge localization in the direction of the pulse polarization and it varies in the interval $[-1, 1]$. When the extremal values -1 and 1 are reached then a perfect localization at the angles $\theta = \pi$ and $\theta = 0$, respectively, is achieved. The dipole moment μ_{m_0} along the x axis corresponding to a particle initially in the m_0 th stationary state is proportional to $\langle \cos \theta \rangle_{m_0}(t)$, i.e.

$$\mu_{m_0}(t) = q\rho_0 \langle \cos \theta \rangle_{m_0}(t). \quad (42)$$

Making use of Eqs. (34) - (36) and (41) we derive the relations

$$\langle \cos \theta \rangle_{m_0}(t) = \Theta(t) \alpha h(\Omega) \sin \left[\frac{2\pi t}{\tau_p} \right] \cos \left[\frac{4\pi m_0 t}{\tau_p} \right], \quad (43)$$

$$\Omega = \alpha \sqrt{2 - 2 \cos[4\pi t/\tau_p]} \quad ; \quad \tau_p = \frac{4\pi m^* \rho_0^2}{\hbar}, \quad (44)$$

and

$$h(\Omega) = J_0(\Omega) + J_2(\Omega). \quad (45)$$

The total dipole moment induced along the x axis by application of an HCP is

$$\mu(t) = \sum_{m_0, \sigma} f(m_0, t) \mu_{m_0}(t). \quad (46)$$

Here σ is the spin of the particle, f is the non-equilibrium distribution function, and $\mu_{m_0}(t)$ is given by Eq. (42).

4.1.1. Numerical results

For a demonstration of the HCP-induced polarization let us consider a ballistic GaAs-AlGaAs ring similar to that used in the experiment reported in Ref. [15]. We assume the ring width is $d \ll \lambda_F$ so that only the lowest radial channel is relevant. The ring radius is $\rho_0 = 1.35 \mu\text{m}$, and the electron effective mass is $m^* = 0.067m_e$, and $N = 1400$. Zero temperature is assumed.

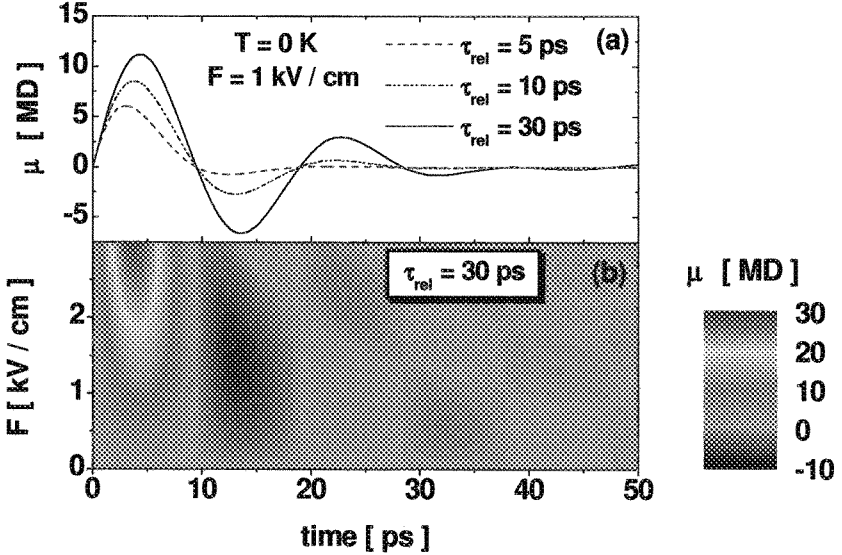


Fig. 6. Time dependence of the dipole moment μ corresponding to the case of spin $\frac{1}{2}$ particles for different values of the relaxation time τ_{rel} (a) and with varying the pulse strength F (b).

Using the relaxation time approximation [31] for the evaluation of the non-equilibrium distribution function we calculate the time dependence of the total dipole moment μ^σ for different values of the relaxation time τ_{rel} Figs. 6 (a). In Figs. 6 (b) the dipole moment is displayed as a density plot as function of the time and the pulse field amplitude $F = F_1$. The duration of the pulse is 1 ps so that the dynamics of the polarization occurs in a field-free manner. Furthermore, the largest polarization is achieved with a magnitude being in the range of several 10^7 D. As to be expected, the induced dipole moment increases with the pulse field strength, even though the time within which the polarization is formed decreases for stronger

fields [see Fig. 6 (b)]. The modulation observed in Fig. 6 (b) point to the possibility of tuning the polarization by an appropriate choice of the applied pulses.

4.2. Pulse induced charge currents

If two linearly polarized pulses are applied to the ring in the way show in Fig. (5) a net time-dependent current $I(t)$ and an associated magnetization is created

$$I(t) = \sum_{l_0, m_0, \sigma} f(l_0, m_0, \sigma, N, T, t) I_{l_0, m_0}(t).$$

Here the radial and angular quantum numbers l_0 and m_0 as well as the spin σ label the initial state from which the current starts and I_{l_0, m_0} is the associated partial current which in its turn is obtained from the time dependent wave function, derived in a similar manner as described in the preceding section (although now we are also including the influence of the radial channels).

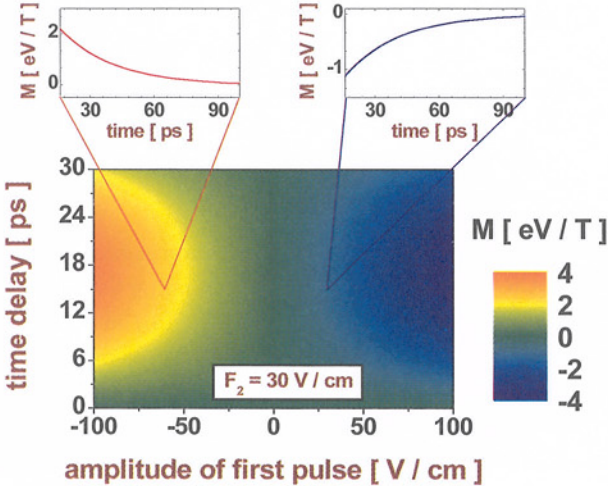


Fig. 7. Induced magnetization M as a function of the time delay τ and the amplitude F_1 of the first pulse. The amplitude of the second pulse is set to the value $F_2 = 30$ V/cm. Positive and negative values of F_1 refer to pulse polarizations in the x and $-x$ directions, respectively. The upper left and right insets show for the time delay $\tau = 15$ ps the time dependence of the magnetization for respectively the field amplitudes of $F_1 = -60$ V/cm and $F_1 = 30$ V/cm. The ring radius is $\rho - 0 = 1350$ nm and its width is $d = 10$ nm. The induced current is inferred by noting that for this ring a magnetization of 1 eV/Tesla corresponds to a current of 8.9 nA.

The HCP induced current results in a time-dependent field-free magnetization $M(t)$. For rings with $d \ll \rho_0$ this dynamic magnetization is given by the classical formula $M(t) \approx \pi \rho_0^2 I(t)$. Fig. (7) shows a prototypical example of the the pulses-induced magnetization in the ring as a function of the delay time τ between the two pulses and as a function of the field amplitude strength F_1 of the first pulse ($F_2 = 30$ V/cm). A net current I of 8.9 nA corresponds in Fig. 7 to a ring magnetization of 1 eV/Tesla. Thus, the induced peak magnetization is an order of magnitude larger than the magnetization measured in mesoscopic rings threaded by a magnetic flux [15] in which case one measures a persistent current of ~ 4 nA. Here we should stress however, that in contrast to persistent currents, the HCP generated currents are non-equilibrium states that generally decay in time, as demonstrated by the insets of Fig. 7 for two peak magnetizations. Nevertheless, as evident from these numerical illustrations the current lasts for almost 100 ps. To maintain the current beyond this time period one should utilize a train of appropriate pulses, as done above for the case of a double quantum well.

The induced magnetization direction is changed by changing the polarity of the first pulse (cf. Fig. 7). Positive or negative polarity of F_1 leads respectively to a charge polarization either along the x or $-x$ directions and this eventually results in a different magnetization direction. In addition to being able to tune the magnetization direction, the peak magnetization value can also be controlled by changing the time lag τ between the pulses.

The numerical results shown in Fig. 8 demonstrate how collective magnetic phases in an artificially structured planar array of rings [21] can be generated and controlled by means of HCPs: The magnetic moment of the individual rings in the array can be varied for changing for example the radii ρ_0 or the particle number N [see Figs. 8(a)-(d)]. In the example shown in Fig. 8 we have however, not yet included the dipole-dipole coupling between the magnetization of the rings, for we assume the distance between the rings to be large for the dipolar interaction to be effective. For closer packed rings such interaction effects are expected to be quite important. A study of this case is however still outstanding.

5. Pulse-induced electron removal from a quantum dot

As a final example we consider the electron removal from a semiconductor quantum dot upon irradiation with a half-cycle pulse. A quantum dot, also called a nanocrystal or artificial atom, is a semiconductor crystal having a size on the scale of the carriers wave length and surrounded by another

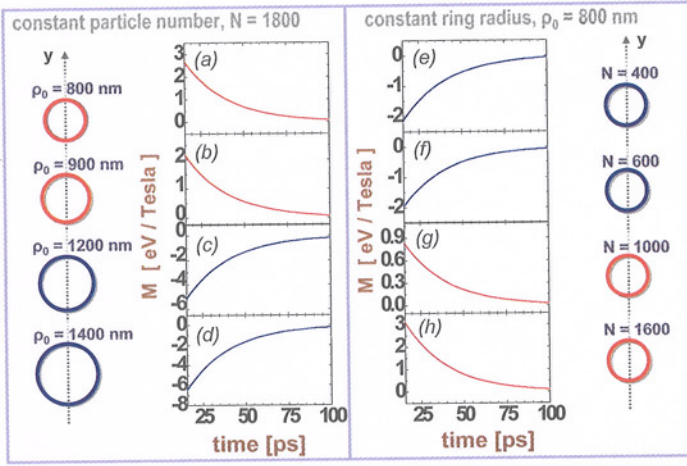


Fig. 8. The time-dependence at $T = 0$ of the magnetization induced by 1 ps pulses in an array of four non-interacting rings with a fixed particle number N and varying radii ρ_0 [(a)-(d)] or with fixed ρ_0 and varying N [(e)-(h)]. All rings are 100 nm wide, the field amplitude strengths are $F_1 = F_2 = 80$ V/cm and the delay time between the pulses is $\tau = 15$ ps.

semiconductor material with a broader band gap. Methods and procedures for the fabrication of quantum dots as well as further physical properties are found in Ref. [32]. The boundary of a quantum dot can be smooth or abrupt. Here we consider the case of an abrupt boundary, modelled by a rectangular energetic wells with finite barrier heights for electrons and holes in all three dimensions. Usually, a quantum dot like an atom has a series of discrete bound energy levels and a continuum band of infinite number of energy levels. Using appropriate semiconductor materials and fabrication procedures, the size and the barrier heights of the quantum dots can be controlled. Quantum dots have two types of carriers, electrons and holes which can recombine with each other. The carriers at the discrete energy levels are spatially confined inside the dot with some tunnelling tails penetrating to the region outside the dot. Here we investigate the probability of transferring the confined carrier which initially resides in a discrete level to the continuum part of the spectrum by the application of a half-cycle pulse.

For simplicity, we consider a spherical quantum dot containing a single discrete electron level (the condition for such a situation will be clarified below) which is occupied before the pulse application. We also assume that electrons of the semiconductor materials inside and outside the quantum dot have simple parabolic isotropic bands determined by the same effective mass

m^* . The radius of the quantum dot will be denoted as R and the energy barrier height as U_e . To render the following equations more transparent we introduce normalized radial coordinate $\tilde{r} = r/R$ and normalized energy barrier height $u = U_e/E_n$ where the normalization energy is given by $E_n = \frac{\hbar^2}{2m^*R^2}$. Solving the Schrödinger equation with the corresponding boundary conditions one finds the equation

$$\lambda j_1(\lambda)k_0(\kappa) - \kappa j_0(\lambda)k_1(\kappa) = 0, \quad (47)$$

determining all discrete energy levels $E = \lambda^2 E_n$ of the system. Here $\kappa = \sqrt{u - \lambda^2}$, $j_l(x)$ denote the spherical Bessel functions of the first kind and $k_l(x)$ denote the modified spherical Bessel functions of the third kind [30] [explicitly, we have $j_0(x) = \sin(x)/x$, $j_1(x) = \sin(x)/x^2 - \cos(x)/x$, and $k_0(x) = \frac{\pi}{2} \exp(-x)/x$, $k_1(x) = \frac{\pi}{2}(x+1)\exp(-x)/x^2$]. Depending on the normalized barrier height u Eq. (47) can have no real solutions or have finite number of real solutions. Generally, the number of discrete levels increases making the values of the confining potential U_e or the dot radius R larger. Both of these factors are combined in the normalized energy barrier height u . One finds that for $u \in ((\pi/2)^2, (3\pi/2)^2)$ there is exactly one discrete electron level in the dot. The wave function is given by

$$\begin{aligned} \psi(\tilde{r}) &= C_{\text{in}} j_0(\lambda \tilde{r}), & \tilde{r} \leq 1; \\ \psi(\tilde{r}) &= C_{\text{out}} k_0(\kappa \tilde{r}), & \tilde{r} > 1; \end{aligned} \quad (48)$$

where $C_{\text{out}} = C_{\text{in}} j_0(\lambda)/k_0(\kappa)$ and

$$C_{\text{in}} = \left[\frac{2\pi}{\lambda^2} (1 - j_0(2\lambda)) + \frac{2\pi}{\kappa} j_0^2(\lambda) \right]^{-1/2}. \quad (49)$$

When the half-cycle pulse duration σ satisfies the following condition

$$\sigma \ll \frac{\hbar}{(u - \lambda^2) E_n} \quad (50)$$

the impulsive approximation can be applied and we find the wave function right after the pulse application using the matching given by Eq. (13). The probability P_0 for an electron to stay at the level inside the dot after the excitation is given by the absolute value square of the projection of the wave function after the pulse application onto the unperturbed wave function of the quantum dot level,

$$P_0(\tilde{p}) = \left| \int d^3\tilde{r} |\psi(\tilde{r})|^2 e^{i\tilde{p}\tilde{r}} \right|^2 = \left| \frac{4\pi}{\tilde{p}} \int_0^\infty r d\tilde{r} |\psi(\tilde{r})|^2 \sin(\tilde{p}\tilde{r}) \right|^2, \quad (51)$$

where $\tilde{p} = pR/\hbar$ with p being the transferred momentum. The probability of quantum dot ionization is $P_{\text{ion}} = 1 - P_0$. The analytic expression for

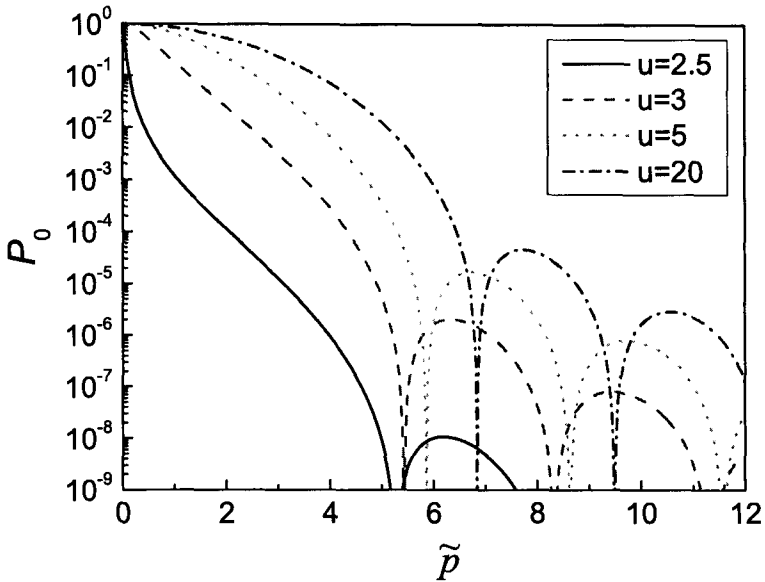


Fig. 9. Dependence of the probability P_0 to stay at the discrete level after the excitation by a half-cycle pulse on the normalized transferred momentum \tilde{p} .

$P_{\text{ion}}(\tilde{p})$ is too cumbersome, therefore, we do not give it here but illustrate this dependence in Fig. 9 for several values of the barrier height. We see from this figure that for efficient ionization of shallow levels, weaker pulses are required than for the case of deeper levels. Adjusting the pulse strength it is possible to achieve complete ionization of the quantum dot level.

6. conclusions

We discussed in this work the use of short asymmetric electromagnetic pulses for tracing and controlling the electron dynamics in double quantum well structures and mesoscopic rings. Using analytical and numerical analysis we demonstrate how charge polarization and charge currents can be created in the rings on a picosecond time scale and how these physical phenomena can be modified in a controllable way by changing the parameters of the external driving fields. We also discuss the possibility of HCP-induced electron removal from quantum dots.

References

1. T. Brabec and F. Krausz, Rev. Mod. Phys. 72, 545 (2000)

2. J.-C. Diels, W. Rudolph, *Ultrashort Laser Pulse Phenomena* (Academic Press, New York, 1996).
3. R. R. Jones, D. You, and P. H. Bucksbaum, *Phys. Rev. Lett.* **70**, 1236 (1993); R.R. Jones, *ibid* **76**, 3927 (1996); N.E. Tielking, R.R. Jones, *Phys. Rev. A* **52**, 1371 (1995); J. G. Zeibel, R. R. Jones, *ibid* **68**, 023410 (2003); D. You, R. R. Jones, and P. H. Bucksbaum, *Opt. Lett.* **18**, 290 (1993); C. O. Reinhold, J. Burgdörfer, M. T. Frey, and F. B. Dunning, *Phys. Rev. Lett.* **79**, 5226 (1997); M. T. Frey, F. B. Dunning, C. O. Reinhold, S. Yoshida, and J. Burgdörfer, *Phys. Rev. A* **59**, 1434 (1999); S. Yoshida, C. O. Reinhold, and J. Burgdörfer, *Phys. Rev. Lett.* **84**, 2602 (2000); B. E. Tannian, C. L. Stokely, F. B. Dunning, C. O. Reinhold, S. Yoshida, and J. Burgdörfer, *Phys. Rev. A* **62** (2000) 043402.
4. N. E. Tielking, T. J. Bensky, and R. R. Jones, *Phys. Rev. A* **51**, 3370 (1995).
5. N. E. Henriksen, *Chem. Phys. Lett.* **312**, 196 (1999).
6. A. Matos-Abiague and J. Berakdar, *Appl. Phys. Lett.* **84**, 2346 (2004); *Phys. Rev. B* **69** 155304 (2004).
7. Y. Imry, *Introduction to mesoscopic physics*, 2nd. edition (University press, Oxford, 2002).
8. M. Büttiker, Y. Imry, and R. Landauer, *Phys. Lett. A* **96**, 365 (1983).
9. R. Landauer and M. Büttiker, *Phys. Rev. Lett.* **54**, 2049 (1985).
10. H. F. Cheung, Y. Gefen, E. K. Riedel, and W. H. Shih, *Phys. Rev. B* **37**, 6050 (1988).
11. J. F. Weisz, R. Kishore, and F. V. Kusmartsev, *Phys. Rev. B* **49**, 8126 (1994).
12. W. C. Tan and J. C. Inkson, *Phys. Rev. B* **60**, 5626 (1999).
13. D. Loss and P. Goldbart, *Phys. Rev. B* **43**, 13762 (1991).
14. S. A. Washburn and R. A. Webb, *Add. Phys.* **35**, 375 (1986).
15. D. Mailly, C. Chapelier, and A. Benoit, *Phys. Rev. Lett.* **70**, 2020 (1993).
16. A. Müller-Groeling and H. A. Weidenmüller, *Phys. Rev. B* **49**, 4752 (1994).
17. G. Bouzerar, D. Poilblanc, and G. Montambaux, *Phys. Rev. B* **49**, 8258 (1994).
18. T. Chakraborty and P. Pietiläinen, *Phys. Rev. B* **50**, 8460 (1994).
19. L. P. Lévy, G. Dolan, J. Dunsmuir, and H. Bouchiat, *Phys. Rev. Lett.* **64**, 2074 (1990).
20. V. Chandrasekhar, R. A. Webb, M. J. Brady, M. B. Ketchen, W. J. Gallagher, and A. Kleinsasser, *Phys. Rev. Lett.* **67**, 3578 (1991).
21. W. Rabaud, L. Saminadayar, D. Mailly, K. Hasselbach, A. Benoît, and B. Etienne, *Phys. Rev. Lett.* **86**, 3124 (2001).
22. K. B. Efetov, *Phys. Rev. Lett.* **66**, 2794 (1991).
23. V. E. Kravtsov and V. I. Yudson, *Phys. Rev. Lett.* **70**, 210 (1993).
24. O. L. Chalaev and V. E. Kravtsov, *Phys. Rev. Lett.* **89**, 176601 (2002).
25. P. Kopietz and A. Völker, *Eur. Phys. J. B* **3**, 397 (1998).
26. M. Moskalets and M. Büttiker, *Phys. Rev. B* **66**, 245321 (2002).
27. K. Yakubo and J. Ohe, *Physica E* **18**, 97 (2003).
28. G. M. Genking and G. A. Vugalter, *Phys. Lett. A* **189**, 415 (1994).
29. A. Matos-Abiague and J. Berakdar, *Phys. Rev. Lett.* **94**, 166801/1-4 (2005); *Europhysics Letters* **69**, 277-283 (2005); *Phys. Rev. B* **70**, 195338/1-10

- (2004).
30. M. Abramowitz and I. Stegun (Eds.), *Handbook of Mathematical functions*, Dover Publications, New York, 1972.
 31. J. M. Ziman, *Principles of the Theory of Solids*, Scnd. edition (University press, Cambridge, 1998); W. Jones and N. H. March, *Theoretical Solid State Physics*, Vol. 2 (Dover Publications, New York, 1985).
 32. P. Harrison, *Quantum Wells, Wires and Dots*, Wiley, New York, 2001.